*Engineering Transactions*, **73**(3): 463–483, 2025, https://doi.org/10.24423/engtrans.3498.2025
Institute of Fundamental Technological Research Polish Academy of Sciences (IPPT PAN)
Université de Lorraine • Poznan University of Technology

# SiMRTRANS

# Analysis of a Variable Geometry Radial Inflow Turbine Using 1D Mean-line Model

Dmytro SAMOILENKO

*Faculty of Automotive and Construction Machinery Engineering*
*Warsaw University of Technology*
Warsaw, Poland

e-mail: dmytro.samoilenko@pw.edu.pl

Despite great progress in 3D computational fluid dynamics (CFD), mathematical modeling used for turbomachinery analysis, the prediction of flow parameters in the rotor (impeller) of radial inflow turbines using existing turbulence models often yields unsatisfactory results. This is because real physical processes related to turbulence are very complex. Other limitations of CFD tools include numerical errors due to finite difference approximations. Thus, for the analysis and optimization of radial inflow turbines, empirical loss correlations applied to a mean-line 1D mathematical model can provide faster and more accurate results compared to CFD simulations. In this study, a 1D approach was used for the mathematical modeling of gas flow in a variable geometry radial inflow turbine with a vaneless volute distributor (VVD). The variable geometry turbine (VGT) was part of a turbocharging system. Combustion engine operation mode with high-power and low-crankshaft rotational speed was chosen, as engine performance under this condition is sensitive to turbocharger adjustment in terms of break specific fuel consumption (BSFC) and other critical parameters. An experimentally-based approach was used where gas flow characteristics in the VGT were calculated under real engine-turbocharger operating conditions. Accordingly, exhaust gas parameters were first measured on an experimental setup. Mathematical modeling then allowed to assess how adjustment in VGT influenced turbine indices, including loss distribution across the stage. It was also validated in this study that during high-load and low-crankshaft operating conditions of the compression ignition (CI) engine, it is recommended to minimize the cross-sectional area at the outlet of the volute acceleration section in the VGT. This adjustment results in better fuel efficiency and lower thermal loads on turbine components, despite a slight reduction in the turbine's overall efficiency.

**Keywords:** mathematical modeling; radial inflow turbine; variable geometry; loss analysis.



## List of abbreviations and symbols

1D – one-dimensional,
3D – three-dimensional,
$A$ – cross-sectional area at the outlet of the volute acceleration section, mm$^2$,

BSFC – break specific fuel consumption, g/kW,
CFD – computational fluid dynamics,
CI – compression ignition,
EGR – exhaust gas recirculation,
FCAS – fuel cell air supply system,
ICE – internal combustion engine,
$\lambda$ – air excess factor,
RIT – radial inflow turbine,
VGT – variable geometry turbine,
VVD – vaneless volute distributor,
$\eta_{\text{turbo}}$ – turbocharger efficiency,
$\eta_{ec}$ – compressor efficiency,
$\eta_{et}$ – turbine efficiency.

## 1. Introduction

Currently, the core areas of applications of radial inflow turbines (RITs) are turbocharging systems for internal combustion engines (ICEs), expanders used in organic rankine cycle (ORC) heat recovery solutions [1], and fuel cell air supply systems (FCAS) [2]. The most promising future trends in RIT research and development are solar microturbines [3] and hydrogen turboexpanders [4]. In all of these mentioned solutions, turbine adjustment through variable geometry can improve performance of the system by maintaining high overall efficiency under both steady-state and transient operating modes. In this context, an effective tool is needed for the analysis and optimization of variable geometry radial inflow turbines. A mathematical model of a variable geometry RIT, capable of simulating gas flow in the turbine stage and calculating losses in its components can serve this purpose.

In the theory of turbomachinery, the level of a mathematical model depends on the number of coordinates used to define flow parameters in the internal components of the turbine stage. In a "zero-dimensional" model, only general balances on energy and mass transfer are considered. The turbine is considered a "black box" through which a specified mass of the gas flows and internal losses are considered. Thus, there is no need to associate the process with any coordinates and this model could be referred to as "zero-dimensional".

In 1D mathematical models, the turbine stage is divided into specific zones that are matched. Flow parameters between these zones are averaged as fluid moves from the turbine inlet to the outlet. Cross-sections are established along the axis of the rotor. In this context, the flow parameters depend only on one coordinate. During fluid motion, its thermophysical properties change depending on turbine's design and operating conditions. In a 1D mathematical model of a radial inflow turbine, the following fundamental equations must be solved [5]:

the continuity equation, the energy equation in both thermal and mechanical forms, and the momentum equation. Such mathematical models are also called 1D mean-line codes. These codes allow investigation of how key design parameters affect overall turbine performance in terms of power output and efficiency. Selected results of such investigations can be found in [1–4, 6–8].

In [3], a comparative study on enthalpy loss and the analysis of a cavity-structured radial turbine for solar hybrid microturbine applications was conducted based on a mean-line model. A novel optimization methodology for the preliminary design of hydrogen turboexpanders, integrating the traditional mean-line method with particle swarm optimization, is shown in [4]. In [1], 1D modeling was used for the design and optimization of a radial inflow turbine (expander) developed for application in a low temperature ORC. It was shown in that study that, for fuel cell with a 5 kW electrical output, an additional 0.7 kW could be generated through the use of the ORC. In [7], 1D mean-line modeling combined with CFD analysis were used for designing a small-scale radial turboexpander for ORC applications. Such methodology allowed for investigation of the effects of key design parameters on the overall turbine performance in terms of power output and efficiency. Mean-line analysis was used in turbine designing process where radial turbine was developed for small-scale, low temperature operation based on the thermodynamic ORC with a 10 kW power output [8].

The most popular area of application of radial inflow turbines is in exhaust gas turbocharging systems. Currently, turbocharging has become the preferred approach for downsizing internal combustion engines, aiming to reduce fuel consumption and $CO_2$ emissions [6]. In [6], a mean-line turbine model was used to optimize the design of a fixed-geometry turbine with the goal of minimizing fuel consumption across a given set of engine operating points. Full-load and part-load cases were considered. It was shown that in full-load case, the optimized turbine geometry reduced the average BSFC by 3.5 g/kWh per cycle. Part-load optimized design achieved a 0.9 g/kWh cycle-averaged BSFC improvement. It was rightly pointed out in [6] that in real-world driving cycles for passenger vehicles, most of the time is spent in part-load modes. In another work, unsteady testing conditions in terms of pressure pulses, were investigated for single-entry and twin-entry turbine using the 1D TURBODYNA software [9]. This type of modeling allows evaluating not only turbocharger performance but also conduct turbocharger – engine matching analysis under pulsating flow conditions. Research [10] was devoted to the comparison of loss models used for performance prediction of radial inflow turbine based on 1D mean streamline analysis. An optimal set of loss models was proposed, addressing rotor passage losses and tip clearance losses. It was also highlighted that the 1D mean-line approach, when supported by empirical loss correlations, provides the results of turbine performance analysis with higher accuracy compared to CFD procedures. The reason

is inaccuracy in CFD prediction for the flow field in the rotor. As shown in [11], major errors in CFD-based routine turbomachinery design include: numerical errors due to finite difference approximations, modeling errors where the true physics is not known or is too complex to model (e.g., turbulence modeling), and uncertainties in geometrical parameters such as tip clearances or leading-edge shapes presented in real-world sample. That is why the current study employs a 1D approach for the mathematical modeling of gas flow in a variable geometry radial inflow turbine equipped with a vaneless volute distributor (VVD).

Currently, the majority of research in the field of mathematical modeling of gas dynamic processes in turbines with variable geometry focuses on nozzle ring adjustment. In the current work, an alternative VGT configuration is investigated where adjustment is achieved by varying the cross-sectional area at the outlet of the volute acceleration section. For this purpose, a custom model developed by the author is used. Moreover, a loss analysis of the turbine stage in the VGT equipped with a VVD was conducted under the specific engine operating condition characterized by high-load and low-crankshaft rotational speed. These findings are novel.

## 2. Variable geometry turbine (VGT) with vaneless volute distributor (VVD)

In this research, a prototype of a variable geometry turbocharger with two gas inlets was investigated during its join operation with a V-type CI engine. A 1D approach was used for loss analysis in the VGT equipped with VVD. The core elements of the variable geometry turbine are shown in Fig. 1.

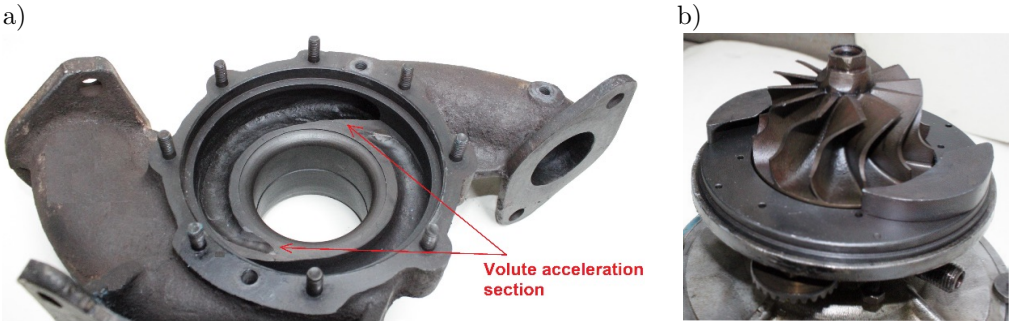


Fig. 1. Prototype of a variable geometry turbocharger: a) turbine housing, b) profiled elements mounted on the rotating disc.

The presented concept is a patented alternative [12] to the traditional nozzle ring adjustment. Here, instead of using a multi-vane nozzle ring, turbine adjustment is achieved through varying the cross-sectional area at the outlet from the

volute acceleration section (Fig. 1a). A specially profiled element mounted on the disc (Fig. 1b) ensures turbine's adjustment. This design allows to control the exhaust gas velocity acting on the turbine's impeller in response to the required compressor pressure. Here, at low engine speeds and high loads, the flow rate through the turbine decreases and the adjusting disk rotates clockwise, ensuring additional acceleration of the gas through the reduced cross-sectional area at the outlet of the volute acceleration section. This causes additional acceleration of the gas flow, which increases the turbocharger shaft speed. As a result, higher boost pressure is generated and an increased amount of air is delivered to the engine cylinders. Thus, an optimal air-fuel ratio is achieved during operation modes with insufficient air supply. At high engine speeds and low loads, the adjusting disk rotates counterclockwise, ensuring increased cross-sectional area at the outlet of the volute acceleration section. This reduces the flow velocity at the impeller inlet and causes the turbine's shaft to decelerate. This leads to lower boost pressure and, consequently, an optimal air-fuel ratio established under low load modes of operation. The position of the profiled element is controlled by an actuator. Selected geometrical parameters of the VGT are shown in Table 1.

Table 1. Selected parameters of the VGT.

| Parameter | Value |
|---|---|
| Inlet radius of the impeller, mm | 42.5 |
| Blade height at the inlet, mm | 11.9 |
| Width of the impeller, mm | 33.3 |
| Inlet angle of the impeller, deg | 90 |
| Outlet angle of the impeller, deg | 30 |
| Root radius of the impeller blade, mm | 12.5 |
| Number of the impeller blades | 12 |
| Root thickness of the impeller blade, mm | 2.45 |
| Shaft diameter, mm | 13 |
| Cross-sectional area at the inlet to the volute, $mm^2$ | 5021 |
| Minimum cross-sectional area at the outlet from the volute acceleration section, $mm^2$ | 1442 |
| Maximum cross-sectional area at the outlet from the volute acceleration section, $mm^2$ | 2312 |
| Diameter at the annular confuser inlet, mm | 109 |
| Diameter at the annular confuser outlet, mm | 87 |

The developed design of the VGT enabled a 40% reduction in the value of $A$ (cross-sectional area at the outlet from the volute acceleration section). This relationship between $A$ and the relative displacement of the profiled elements $\overline{x}$ for the investigated turbine with variable geometry, is shown in Fig. 2.

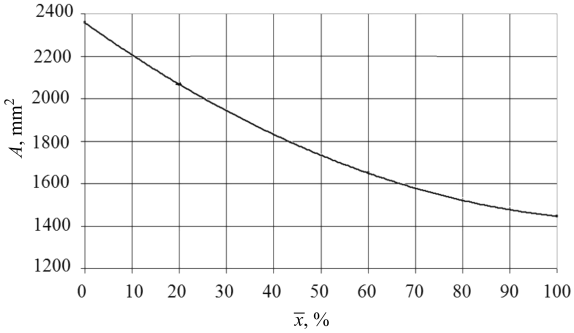


FIG. 2. Relationship between $A$ and relative displacement of the profiled elements $\overline{x}$ in the VGT prototype.

The next stage of the research was devoted to experimental investigation and studying the influence of variable geometry in the turbine on selected parameters of a four-stroke six-cylinder, V-type turbocharged diesel engine.

## 3. Experimental research

### *3.1. Methodology of the research*

A short specification of the CI engine used in experiments is shown in Table 2.

TABLE 2. Experimental CI engine specification.

| Parameter | Value |
|---|---|
| Rated power, kW | 125 |
| Engine speed at rated power, rpm | 2100 |
| Engine type/Number of cylinders | V-type/6 |
| Bore, mm | 130 |
| Stroke, mm | 115 |
| Engine displacement, $dm^3$ | 9.15 |
| Fuel delivery system | Direct injection with BOSCH high-pressure fuel pump |
| Air delivery system | Turbocharger with intercooler |

In the present research, only the influence of turbine adjustment (the variation of the cross-sectional area at the outlet of the volute acceleration section) on diesel engine parameters was investigated. There were no modifications made to the fuel delivery and EGR systems. In the future research, combined turbocharger and EGR technology could be considered. As shown in [13], such a combined approach would allow to drastically reduce $NO_x$, HC, and smoke emissions. Turbocharging increases EGR compatibility by producing a greater

charge mass in the combustion chamber. The following cross-sectional areas at the outlet of the volute acceleration section $A$ were set in the variable geometry turbine: 1442 mm$^2$, 2065 mm$^2$, and 2312 mm$^2$. The minimum and maximum values of $A$ were limited by the possibility of installing adjustment elements in the commercial turbine housing. In the future, redesigning the turbine housing could expand the range of variation in the value of $A$. In this context, even a small reduction in the minimum cross-sectional areas at the outlet of the volute acceleration section (below 1442 mm$^2$) could be beneficial for selected modes of engine operation where $\lambda$ is below 1.6. Performance characteristics of the diesel engine were obtained by registering indices during steady-state operation. These measured parameters were converted into key engine and turbocharger indices, enabling analysis of loss distribution in the VGT during the final stage of the research.

Turbocharger efficiency was calculated by an empirical formula [14]:

$$\eta_{\text{turbo}} = 1.045 \cdot T_0 \cdot \left( \frac{\pi_S^{0.2857} - 1}{1.119 \cdot T_T} \right) \cdot \left( 1 - \frac{1}{\pi_T^{0.2593}} \right), \tag{3.1}$$

where $T_0$ is the ambient temperature, $T_T$ is the temperature of the exhaust gas at the turbine inlet, $\pi_S$ is the compressor pressure ratio, and $\pi_T$ is the turbine pressure ratio.

Compressor efficiency was defined based on the experimental compressor map.

Turbine efficiency was calculated by the equation:

$$\eta_{et} = \frac{\eta_{\text{turbo}}}{\eta_{ec}}. \tag{3.2}$$

### *3.2. Influence of the cross-sectional area at the outlet of the volute acceleration section A on engine and turbocharger indices*

The turbocharging system is responsible for delivering a sufficient amount of air into the engine cylinder. The amount of air depends on the boost pressure and affects the quality of the combustion process. Under operating modes with high-load and low-crankshaft rotational speeds, significant deterioration in combustion process is observed due to insufficient air supply delivered by the compressor stage of an improperly controlled turbocharger. At the same time, these conditions allow to analyze the influence of VGT on engine/turbocharger performance indices. For this reason, the steady-mode with an effective power $P_e = 73.5$ kW (high-load) and crankshaft rotational speed $n = 1300$ rpm (low speed) was chosen for this study. The main diesel engine and turbocharger parameters obtained in the experimental research under these conditions are presented in Table 3. Selected results from Table 3 were used as input data for mathematical modeling

Table 3. Performance indices of the experimental CI engine equipped with a VGT turbocharger at a load of $P_e = 73.5$ kW and engine speed $n = 1300$ rpm ($T_0 = 291$ K; $p_0 = 99\,459$ Pa).

| Engine indices | | | | |
|---|---|---|---|---|
| Parameter | Symbol | Cross-sectional area at the outlet of the volute acceleration section $A$, mm$^2$ | | |
| | | $A = 2312$ | $A = 2065$ | $A = 1442$ |
| Break specific fuel consumption, g/kWh | BSFC | 241.4 | 238.9 | 234.8 |
| Air excess factor | $\lambda$ | 1.63 | 1.68 | 1.796 |
| Air mass flow rate through the compressor, kg/s | $G_s$ | 0.116 | 0.118 | 0.123 |
| Boost pressure, kPa | $p_s$ | 120.0 | 123.1 | 127.9 |
| Absolute pressure at compressor inlet, kPa | $p_a$ | 98.4 | 98.3 | 98.1 |
| Exhaust gas pressure at turbine inlet, kPa | $p_T$ | 121.1 | 124.5 | 129.9 |
| Exhaust gas temperature at turbine inlet, K | $T_T$ | 893.7 | 849 | 829.9 |
| Exhaust gas pressure at turbine outlet, kPa | $p_{0T}$ | 101 | 100.64 | 100.6 |
| Exhaust gas temperature at turbine outlet, K | $T_{0T}$ | 745 | 696 | 681.4 |
| Turbocharger efficiency | $\eta_{\text{turbo}}$ | 0.445 | 0.459 | 0.445 |
| Turbocharger rotor speed, rpm | $n_T$ | 40 050 | 43 030 | 45 076 |
| Compressor efficiency | $\eta_{ec}$ | 0.63 | 0.64 | 0.645 |

of gas dynamics processes in VGT, which enabled the loss analysis conducted at the final stage of the current research.

Figure 3 shows the relationships between selected engine parameters and the cross-sectional area at the outlet from the volute acceleration section plotted based on the parameters presented in Table 3.

As it can be seen on Fig. 3, a reduction in the value of $A$ during steady engine operating mode with $P_e = 73.5$ kW and $n = 1300$ rpm resulted in the increased inlet boost pressure $p_s$, and consequently, and $\lambda$ increased from 1.63 to 1.796. The increased amount of fresh charge inside the engine cylinder resulted in improvement of the combustion process (in terms of its completeness) and, consequently, in BSFC reduction by 6.6 g/kWh. It could be also observed that the exhaust gas temperature at the turbine inlet decreased by 63.8 K. Thus, the thermal conditions for the turbine's components were improved. Therefore, it can be concluded that for high-load and low-crankshaft rotational speeds, it is recommended to set the cross-sectional area $A$ to its minimum value in the VGT.

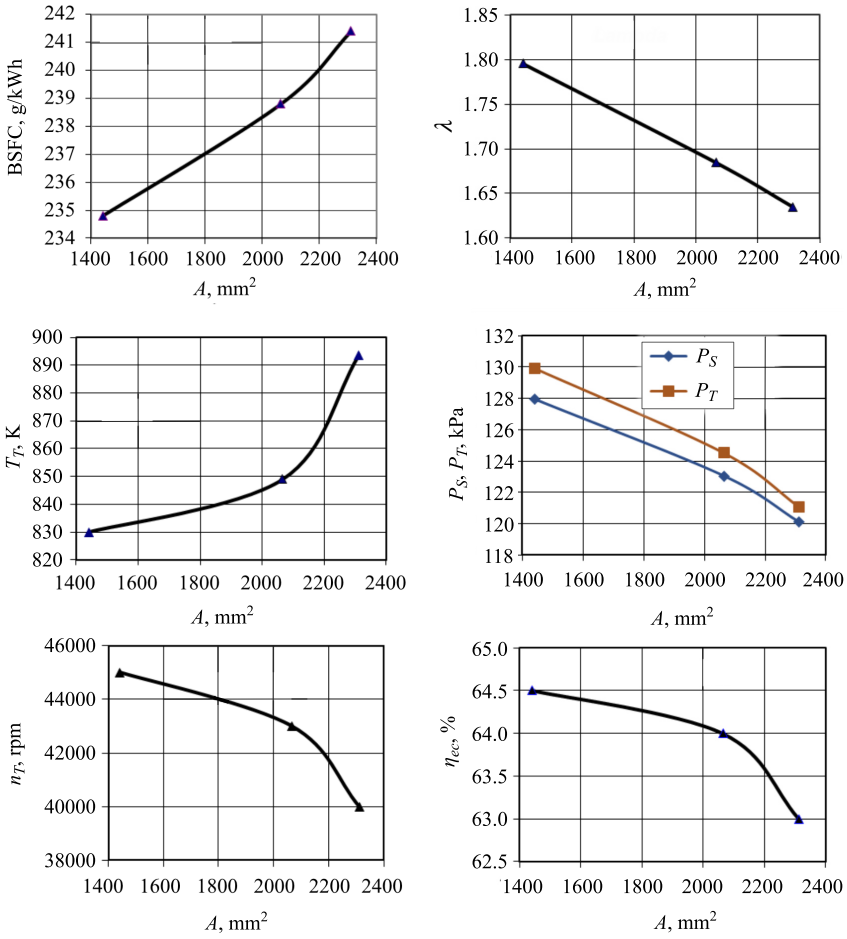


FIG. 3. Dependence of selected indices of experimental engine on the cross-sectional area $A$ during the engine operating mode with with $P_e = 73.5$ kW and $n = 1300$ rpm.

This adjustment brings better fuel efficiency and lower thermal loads on turbine components.

## 4. Mathematical modeling of gas flow in variable geometry radial inflow turbine

### *4.1. The concept of the mathematical model*

Mathematical modeling of gas flow in a radial inflow turbine with a VVD is a key tool for loss analysis in the turbine stage, especially during its adjustment. To improve the accuracy of the model, an experimentally-based approach was taken in the current study where a minimal set of measured data is used.

Constant and variable geometrical parameters of VGT were also incorporated as inputs. A previously developed 1D mean-line mathematical model of the variable geometry radial inflow turbine with VVD [5] was used in this study. A flowchart of the model adapted for the current research is shown in Fig. 4.

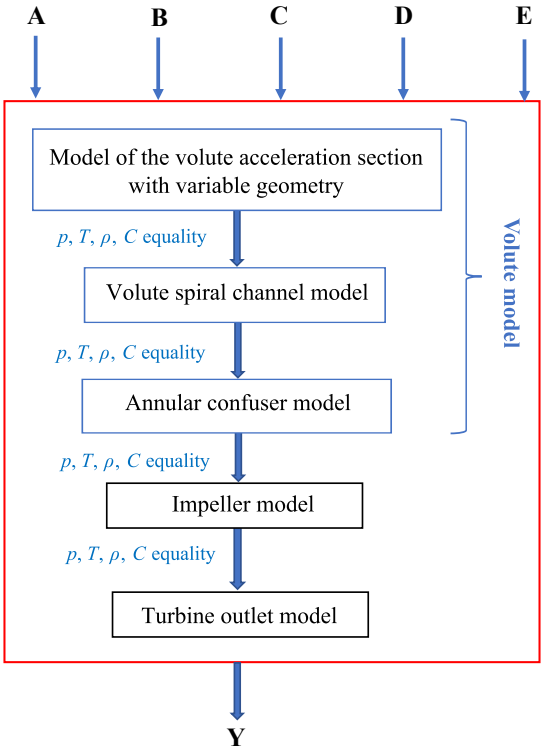


FIG. 4. Flowchart of the mathematical model for a variable geometry radial inflow turbine with a VVD.

The main function of the model is expressed as:

$$Y = f(A, B, C, D, E), \tag{4.1}$$

where $Y$ $(Y_1, Y_2, ..., Y_n)$ is the vector of output parameters, $A$ $(A_1, A_2, ..., A_n)$ is the vector of constant (fixed) geometric parameters, $B$ $(B_1, B_2, ..., B_n)$ is the vector of variable geometric parameters, $C$ $(C_1, C_2, ..., C_n)$ is the vector of input parameters measured during experiments, $D$ $(D_1, D_2, ..., D_n)$ is the vector of the empirical dependencies, and $E$ $(E_1, E_2, ..., E_n)$ is the vector of physical constants.

The mathematical model of the turbine stage includes sub-models for the volute, impeller, and outlet diffuser (Fig. 4). Moreover, the volute model is subdivided into the acceleration section (where variable geometry occurs), the

fixed-geometry spiral channel, and the annular confuser model. Calculations are carried out in a way that turbine stage is divided into computational zones, arranged according to the previously described five sub-models. These zones are matched by ensuring equality of fluid flow parameters at their boundaries. These parameters are pressure $p$, temperature $T$, density $\rho$, and absolute velocity $C$. The fluid is defined as exhaust gas from a CI engine.

### *4.2. Mathematical modeling procedure*

The crucial steps in the calculation procedure are shown in Fig. 5. Firstly, fixed and variable geometric parameters were defined for the turbine stage. 3D models of the volute with variable geometry, where profiled elements located in the position that corresponds to the minimum value of $A$ (1442 mm$^2$) and the maximum value of $A$ (2312 mm$^2$), are shown in Fig. 6. Secondly, the following measured exhaust gas parameters were used as inputs: static pressure $p_T$ and temperature $T_T$ at the turbine inlet, static pressure $p_{0T}$ and temperature $T_{0T}$ at the turbine outlet, and rotor rotational speed. The exhaust gas mass

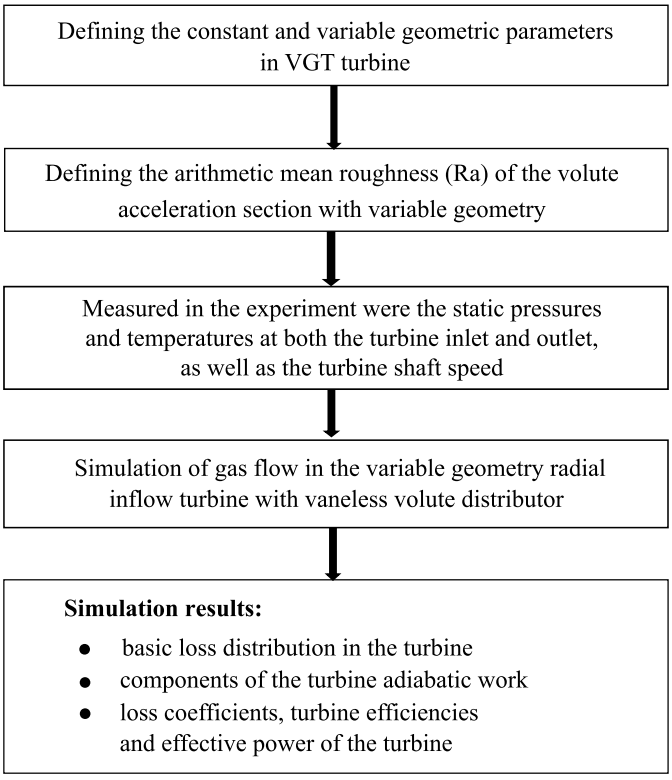


FIG. 5. Flowchart showing the essential steps in the analysis of a variable geometry radial inflow turbine with VVD.

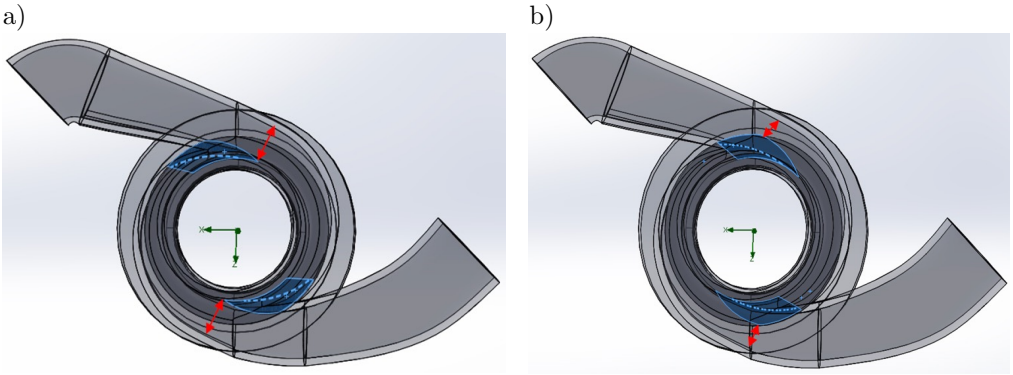


Fig. 6. 3D models of the volute with variable geometry: profiled elements positioned at (a) maximum value of $A = 2312$ mm$^2$ and (b) minimum value of $A = 1442$ mm$^2$.

flow rate was evaluated based on the measured air mass flow rate and fuel mass flow rate. Additionally, an arithmetic mean roughness of the surface for the volute acceleration section was introduced into the mathematical model.

In the flowchart shown in Fig. 5, the most essential step is the last one, which is related to simulation results focused on basic loss distribution for the two critical positions of the profiled element in the VGT.

## 5. Mathematical modeling of gas flow in the variable geometry radial inflow turbine with VVD

In the current study, a 1D mean-line quasi-stationary mathematical model of the variable geometry radial inflow turbine with VVD was used. A detailed description of the model is given in [5]. Further, only the most essential assumptions will be discussed. A schematic diagram of the inflow turbine with VVD is presented in Fig. 7. Here, the following boundaries are considered: turbine inlet (parameters "T"), outlet from the volute acceleration section (parameters "u"), inlet to the turbine impeller (parameters "1"), impeller outlet (parameters "2"), outlet from the turbine's confuser (parameters "0T"). These zones are matched through the equality of the flow parameters at the following boundaries: VVD outlet – impeller inlet, and impeller outlet – turbine confuser inlet.

### *5.1. Model of the VVD with variable geometry*

The VVD consists of the following elements (Fig. 7): acceleration section (position 1), spiral channel (position 2), and annular confuser (position 3). In the current research, the first method described in [5] was used for analysis. This method is based on a 1D approach. As presented in Fig. 8, the average angle

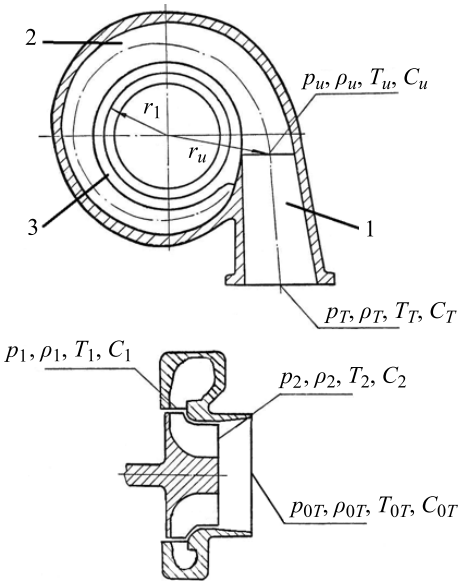


FIG. 7. Simplified layout of the flow section of the radial inflow turbine with VVD [5]: 1 – acceleration section, 2 – spiral channel, 3 – annular confuser.

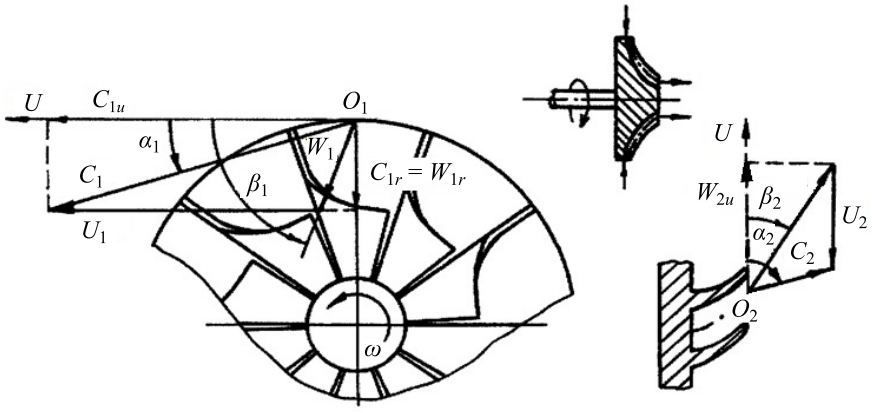


FIG. 8. Velocity diagrams in the turbine impeller [5].

of the gas flow at the outlet from the vaneless distributor in the radial inflow turbine ($\alpha_1$) is calculated using the following semi-empirical relationship:

$$\alpha_1 = \arctan\left[k_u\,(1+\xi_{\mathrm{VVD}})\cdot\frac{\rho_u}{\rho_1}\cdot\frac{A}{2\cdot\pi\cdot r_u\cdot l_1\cdot\cos\alpha_u}\right], \tag{5.1}$$

where $k_u$ is the coefficient that depends on the velocity distribution in the acceleration section. Based on recommendations from [5], $k_u = 0.97$.

Loss coefficient in VVD:

$$\xi_{\mathrm{VVD}} = 0.24 \cdot \left(\frac{10^5}{Re_u}\right)^{0.3} \cdot \left(\frac{r_1}{r_u} \cdot \frac{\cos\alpha_1}{\cos\alpha_u}\right)^2 + 0.0044 \cdot \left(\frac{10^{6-}}{Re_1}\right)^{0.16} \cdot \left[1 - \left(\frac{r_1}{r_u}\right)^{0.84}\right] \cdot \frac{r_1}{l_1 \cdot \sin^2\alpha_1} \cdot \left(\frac{\rho_u}{\rho_1}\right)^{0.3}, \tag{5.2}$$

where Re is the Reynolds number, $\rho$ is the gas density, $r$ is the radii, $\alpha_u$ is the angle between absolute velocity and its tangential component, and $l_1$ is the height of the VVD.

As it can be seen from Eqs. (5.1) and (5.2), variability in the geometric characteristics of the volute acceleration section influences both the angle $\alpha_1$ and losses level in the VVD.

Equations (5.3)–(5.11) were used to calculate the loss components in the turbine stage.

### *5.2. Losses in radial inflow turbine*

Adiabatic work loss in the VVD:

$$l_{rv} = \left(1 - \varphi^2\right) \cdot L_{\mathrm{VVD}}, \tag{5.3}$$

where $\varphi$ is the VVD velocity factor:

$$\varphi = \sqrt{1 - \frac{\zeta_{\mathrm{VVD}}}{1 + \zeta_{\mathrm{VVD}}}}. \tag{5.4}$$

Adiabatic work loss in the impeller:

$$l_{ri} = \left(\frac{1}{\psi^2} - 1\right) \cdot \frac{W_2^2}{2}, \tag{5.5}$$

where $\psi$ is the impeller velocity factor.

Exit energy loss:

$$l_{rc2} = \frac{C_2^2}{2}. \tag{5.6}$$

Turbine rotation loss:

$$l_{fv} = \beta_{fv} \cdot \frac{D_1^2}{G_T} \left(\frac{U_1}{100}\right)^3 \rho_1, \tag{5.7}$$

where $\beta_{fv}$ is the friction and ventilation loss coefficient.

Tip clearance loss:

$$l_{rg} = \xi_{\text{gap}} \cdot \frac{C_0^2}{2}, \tag{5.8}$$

where $\xi_{\text{gap}}$ is the tip clearance loss coefficient, mostly depending on clearance and blade height:

$$\xi_{\text{gap}} = \frac{\delta_2}{h_2 \cdot \sin \beta_2} \cdot L_{adt}. \tag{5.9}$$

Total losses in the turbine:

$$l_{\Sigma t} = l_{rv} + l_{ri} + l_{rc2} + l_{fv} + l_{rg}. \tag{5.10}$$

Indicated work of the turbine:

$$L_i = L_{adt} - l_{\Sigma t}. \tag{5.11}$$

### *5.3. Turbine efficiencies and power output*

Internal efficiency of the turbine:

$$\eta_{ti} = 1 - \frac{l_{\Sigma t}}{L_{adt}}. \tag{5.12}$$

Mechanical efficiency of the turbine:

$$\eta_m = \frac{\eta_{et}}{\eta_{ti}}, \tag{5.13}$$

where $\eta_{et}$ is the effective efficiency of the turbine.

Turbine power output:

$$N_T = G_T \cdot L_{adt} \cdot \eta_{et}. \tag{5.14}$$

## 6. Loss analysis in variable geometry inflow turbine with VVD

Based on the flowcharts shown in Figs. 4 and 5, the influence of adjustment in the VGT on turbine indices, including losses in the turbine stage, was investigated. Exhaust gas parameters were taken for the engine operating mode with $P_e = 73.5$ kW and $n = 1300$ rpm. For this combined engine-turbocharger operating mode, two positions of the profiled element were chosen. These corresponded to the minimum and maximum values of the cross-sectional area at the

outlet of the volute acceleration section ($A = 1442\ \text{mm}^2$ and $A = 2065\ \text{mm}^2$). The basic fixed geometry parameters of the VGT that were used in the mathematical modeling are presented in Table 4.

Table 4. Fixed geometry parameters of the VGT.

| Parameter | Symbol | Value |
|---|---|---|
| Outlet diameter of the impeller, m | $D_1$ | 0.085 |
| Angle at the outlet from the impeller, deg | $\beta_2$ | 30 |
| Operational gap between impeller blades and turbine housing | $\delta_2$ | 0.5 |
| Blade height, mm | $h_2$ | 11 |
| Degree of reaction | $r$ | 0.65 |

Selected experimentally obtained parameters of exhaust gas used for mathematical modeling were taken from Table 3 and are shown in Table 5.

Table 5. Exhaust gas parameters used for mathematical modeling.

| Parameter | Symbol | Cross-sectional area at the outlet from the volute acceleration section $A$, mm$^2$ | |
|---|---|---|---|
| | | $A = 2315$ | $A = 1442$ |
| Absolute pressure at turbine inlet, kPa | $p_T$ | 121.1 | 129.9 |
| Temperature at turbine inlet to the turbine, K | $T_T$ | 893.7 | 829.9 |
| Absolute pressure at turbine outlet, kPa | $p_{0T}$ | 101 | 100.6 |
| Temperature at turbine outlet, K | $T_{0T}$ | 745 | 681.4 |

Main results of the mathematical modelling of gas flow in the variable geometry radial inflow turbine with VVD are presented in Table 6.

Data from Table 6 was used to calculate the losses in the turbine stage, as well as turbine efficiency and power output. These results are presented in Table 7.

Finally, the results of computations allowed for the analysis of the influence of adjustment (through variable geometry) in the radial inflow turbine with a VVD on the following:

- the distribution of losses in the turbine stage,
- the available adiabatic work,
- the loss coefficients of the impeller and VVD,
- the internal efficiency and effective power of the turbine.

TABLE 6. Results of mathematical modeling of gas flow in the variable geometry radial inflow turbine with VVD.

| Parameter | Symbol | Cross-sectional area at the outlet from the volute acceleration section $A$, mm$^2$ | |
|---|---|---|---|
| | | $A = 2315$ | $A = 1442$ |
| Exhaust gas mass flow rate, kg/s | $G_T$ | 0.121 | 0.128 |
| Absolute velocity of gas at turbine inlet, m/s | $C_T$ | 65.0 | 59.9 |
| Stagnation pressure of gas at turbine inlet, kPa | $P_T^*$ | 121.1 | 129.9 |
| Stagnation temperature of gas at turbine inlet, K | $T_T^*$ | 895.5 | 831.5 |
| Adiabatic index for VVD processes | $k$ | 1.349 | 1.356 |
| Available adiabatic work in VVD, J/kg | $L_{\mathrm{VVD}}$ | 27 530.9 | 34 803.3 |
| Degree of reaction | $\rho$ | 0.435 | 0.429 |
| Velocity factor for VVD | $\varphi$ | 0.971 | 0.946 |
| Angle of the flow at the outlet from VVD, deg | $\alpha_1$ | 18.5 | 16 |
| Absolute velocity at VVD outlet, m/s | $C_1$ | 227.8 | 249.6 |
| Blade velocity at impeller inlet, m/s | $U_1$ | 178.0 | 200.3 |
| Tangential component of relative velocity (impeller inlet), m/s | $W_1$ | 81.7 | 79.4 |
| Flow inlet angle in relative motion, deg | $\beta_1$ | 62.2 | 60.05 |
| Impeller velocity factor | $\psi$ | 0.87 | 0.874 |
| Absolute velocity at impeller outlet, m/s | $C_2$ | 80.2 | 87.1 |
| Blade velocity at impeller outlet diameter $D_2$, m/s | $U_2$ | 163.3 | 183.8 |
| Tangential component of relative velocity at impeller outlet, m/s | $W_2$ | 182.7 | 200.0 |
| Absolute velocity at turbine outlet, m/s | $C_{0T}$ | 42.08 | 40.9 |
| Available adiabatic work in turbine, J/kg | $L_{adt}$ | 48 734.4 | 61 002.4 |
| Adiabatic velocity of exhaust gas flow, m/s | $C_0$ | 312.2 | 349.3 |
| U/C ratio | – | 0.56 | 0.57 |

TABLE 7. Losses, efficiency, and power output in the turbine stage.

| Parameter | Symbol | Cross-sectional area at the outlet from the volute acceleration section $A$, mm$^2$ | |
|---|---|---|---|
| | | $A = 2315$ | $A = 1442$ |
| Adiabatic work loss in the VVD, J/kg | $l_{rv}$ | 1570.9 | 3659.1 |
| Adiabatic work loss in the impeller, J/kg | $l_{ri}$ | 5723.3 | 6555.2 |
| Turbine rotation loss, J/kg | $l_{fv}$ | 844.5 | 1264.4 |
| Gas leakage losses, J/kg | $l_{rg}$ | 1476.1 | 1891.1 |
| Total losses in the turbine, J/kg | $l_{\Sigma m}$ | 12 834.4 | 17 162.0 |
| Internal efficiency of the turbine | $\eta_{ti}$ | 0.737 | 0.719 |
| Overall efficiency of the turbine | $\eta_{et}$ | 0.707 | 0.69 |
| Turbine power output, kW | $N_m$ | 4.16 | 5.4 |

The main results of the calculations are shown in Figs. 9 and 10.

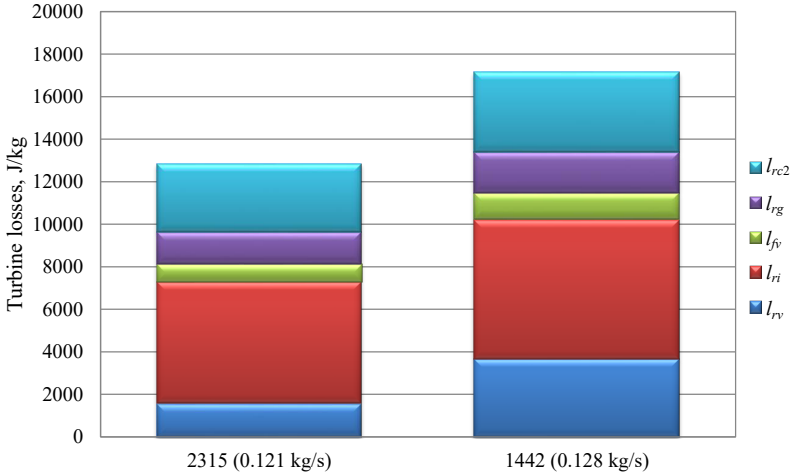


FIG. 9. Distribution of basic loss in the turbine stage: $l_{rc2}$ is the exit energy loss, $l_{rg}$ is the gas leakage loss, $l_{fv}$ is the turbine rotation loss, $l_{ri}$ is the adiabatic work loss in the impeller, $l_{rv}$ is the adiabatic work loss in the VVD.

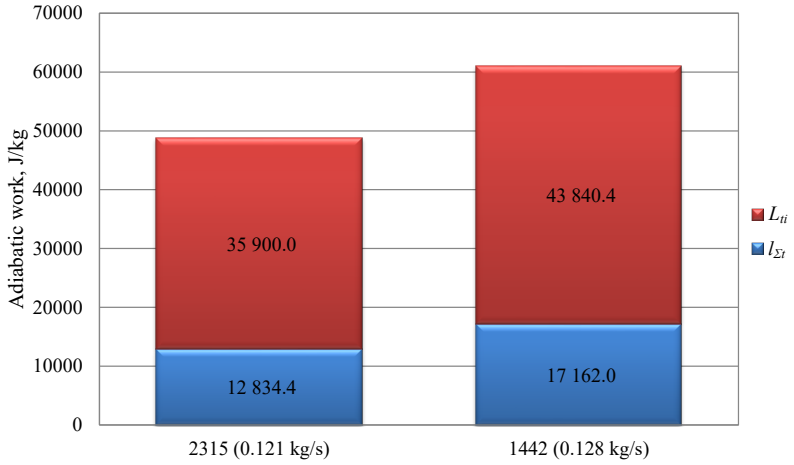


FIG. 10. Adiabatic work distribution in the turbine stage: $L_{ti}$ indicates work of the turbine, $l_{\Sigma t}$ is the total losses in the turbine.

## 7. Conclusions

The following conclusions are drawn from the presented study:

1) Analysis of the results presented in Table 7 and in Figs. 9 and 10 shows that under the diesel engine operation mode with $P_e = 73.5$ kW and

$n = 1300$ rpm, adjusting the turbine by reducing the cross-section $A$ from 2315 to 1442 mm$^2$ leads to a 29.8% increase in power output. This increased power output resulted in higher boost pressure, and a greater amount of air delivered to the engine cylinder. At the same time, total losses in the turbine stage increased by 4327.6 J/kg. The additional power developed by the turbine following the reduction in cross section $A$ can be explained by a positive difference between the increased indicated power (by 7940.4 J/kg) and the increased total losses in turbine stage (by 4327.6 J/kg). Furthermore, the change in the cross-sectional area at the outlet of the volute acceleration section from the maximum (2315 mm$^2$) to the minimum (1442 mm$^2$) also resulted in a slight reduction in the internal efficiency of the turbine when $A = 1442$ mm$^2$ (Table 7). This decreased internal efficiency of the turbine is the result of the less optimal mean flow angle at the outlet of the VVD ($\alpha_1 = 16^\circ$), which is accomplished by a the less beneficial distribution of the velocities at the inlet of the turbine impeller.

2) It was also validated in this study that despite a slight reduction in the turbine's overall efficiency, it is recommended to set the minimum value of the cross-sectional area $A$ in the variable geometry turbine during high-load and low-crankshaft rotational speeds of a CI engine. This will result in better fuel efficiency and lower thermal stress on turbine's components. Thus, shifting the VGT from the maximum to the minimum cross-sectional area $A$ led to a reduction in BSFC by 6.6 g/kWh and a lower exhaust gas temperature at the turbine inlet by 63.8 K.
3) The 1D mean-line model of the variable geometry radial inflow turbine with a VVD can be considered a key tool for loss analysis in the turbine stage. To improve the accuracy of this model, a basic set of parameters should be measured in experiment, including exhaust gas pressures and temperatures at the turbine inlet and outlet, as well as the rotational speed of the turbine rotor.
4) The obtained results can be used for radial inflow turbine's analysis and optimization. The developed mathematical model of a variable geometry radial inflow turbine with a VVD enables not only the investigation of losses in turbocharger turbine stages, but also its adaptation to other applications, including the analysis of expanders in ORC heat recovery systems, optimization of fuel cell recuperation turbines as well as analysis and optimization of hydrogen turboexpanders.
5) In the current research, the average angle of the gas flow at the outlet from of the vaneless distributor in the radial inflow turbine was calculated based on a semi-empirical relationship. For higher accuracy of calculations,

this angle could be established based on 3D CFD simulations conducted according to the methodology presented in [5]. Since the volute with VVD is a static component of the turbine, majority of drawbacks of CFD modeling, as mentioned in the abstract, are significantly minimized in this case.

6) Potential further research involves applying 1D mean-line model of the variable geometry radial inflow turbine with a VVD to analyze the efficiency of energy conversion processes in fuel cell exhaust system turbines.

## References


1. Symes R., Djaname T.N., Deligant M., Sauret E., Design and optimization of a radial inflow turbine for use with a low temperature ORC, *Energies*, **14**(24): 8526, 2021, https://doi.org/10.3390/en14248526.

2. Zhang Y., Xu S., Lin C., Performance improvement of fuel cell systems based on turbine design and supercharging system matching, *Applied Thermal Engineering*, **180**: 115806, 2020, https://doi.org/10.1016/j.applthermaleng.2020.115806.

3. Arifin M., Fudholi A., Schatz M., Vogt D.M., A comparative study of mean-line models based on enthalpy loss and analysis of a cavity-structured radial turbine for solar hybrid microturbine applications, *Energy Conversion and Management*, **287**: 117075, 2023, https://doi.org/10.1016/j.enconman.2023.117075.

4. Che X., Li H., Zhang Z., Chen Y., Cai B., Liu K., Cai W., A novel optimum design method and performance analysis of cryogenic hydrogen turbo-expander for hydrogen liquefaction, *Cryogenics*, **145**: 103996, 2025, https://doi.org/10.1016/j.cryogenics.2024.103996.

5. Samoilenko D., *Variable Geometry Radial Inflow Turbines with Vaneless Distributor: Theory, Research and Application*, Oficyna Wydawnicza Politechniki Warszawskiej, Warszawa, 2019.

6. Kapoor P., Costall A., Sakellaridis N., Hooijer J., Lammers R., Tartoussi H., Guilain S., Adaptive turbo matching: Radial turbine design optimization through 1D engine simulations with meanline model in-the-loop, *SAE Technical Paper*, 2018-01-0974, 2018, https://doi.org/10.4271/2018-01-0974.

7. Rahbar K., Mahmoud S., Al-Dadah R., Mean-line modeling and CFD analysis of a miniature radial turbine for distributed power generation systems, *International Journal of Low-Carbon Technologies*, **11**(2): 157–168, 2016, https://doi.org/10.1093/ijlct/ctu028.

8. Shadreck M.S., Freddie L.I., Radial turbine preliminary design and modelling, *International Journal of Engineering Research & Technology*, **6**(10): 409–415, 2017.

9. Yang B., Shu M., Martinez-Botas R., Yang M., TURBODYNA: A generic one-dimensional dynamic simulator for radial turbomachinery, *Journal of Engineering for Gas Turbines and Power*, **144**(9): 091002, 2022, https://doi.org/10.1115/1.4055018.

10. Cho S.K., Lee J., Lee J.I., Comparison of loss models for performance prediction of radial inflow turbine, *International Journal of Fluid Machinery and Systems*, **11**(1): 97–109, 2018, https://doi.org/10.5293/IJFMS.2018.11.1.097.

11. Denton J.D., Some limitations of turbomachinery CFD, [in:] *Proceedings of the ASME Turbo Expo 2010: Power for Land, Sea, and Air. Volume 7: Turbomachinery, Parts A, B, and C*, Glasgow, UK, June 14–18, 2010, pp. 735–745, https://doi.org/10.1115/GT2010-22540.

12. Petrosyancz V.A., Karnauxov Y.Y., Marchenko A.P., Samojlenko D.E., *Method for adjusting an inflow turbine provided with vaneless distributor*, PCT Patent WO 2006/036134 A1, 2006.

13. Dond D.K., Gulhane N.P., Effect of a turbocharger and EGR on the performance and emission characteristics of a CRDI small diesel engine, *Heat Transfer*, **51**(1): 1237–1252, 2022, https://doi.org/10.1002/htj.22350.

14. Samoilenko D., Marchenko A., Cho H.M., Improvement of torque and power characteristics of V-type diesel engine applying new design of variable geometry turbocharger (VGT), *Journal of Mechanical Science and Technology*, **31**(10): 5021–5027, 2017, https://doi.org/10.1007/s12206-017-0950-2.

*Received December 31, 2024; accepted version July 3, 2025.*
*Online first August 27, 2025.*